Keywords
CAD/CAM, marginal adaptation, differential geometry, zirconia, cement thickness, digital dentistry, internal fit, mesh metrology

Authors
[1]Khageshwar Mandal
Department of Mathematics and Statistics, P.K.M.C., T.U., Nepal
khageshwar.mandal@iost.tu.edu.np

[2]Rishav Jha
Department of Mathemaics, MIT Campus, Janakpurdham, Nepal
jharishav036@gmail.com

[3]Deepak Kumar Mandal
School of Forestry and Natural Resources Management, T.U., Nepal
dpakmandal03@gmail.com

[4*]Suresh Kumar Sahani
Faculty of Science, Technology, and Engineering, Rajarshi Janak University, Janakpurdham, Nepal
sureshsahani@rju.edu.np
Corresponding Author:
sureshsahani@rju.edu.np

Received: 11.104.2026
Revised: 12.05.2026
Accepted: 21.05.2026
Doi: 10.1922/ejprd.v34i2s.1402

A Differential-Geometric Index For Three-Dimensional Crown Adaptation: Implications For Bioactive Cement Distribution And Therapeutic Restorative Interface Optimization

Abstract

Background: HypothyroidismConventional assessment of crown adaptation relies on one- or two-dimensional linear measurements that discard the geometric information inherent in three-dimensional intraoral scan data. This study introduces and validates a novel differential-geometric metric—the Conformal Adaptation Index (CAI)—for quantifying the internal fit of CAD/CAM ceramic crowns, and benchmarks it against simpler three-dimensional comparators.

Materials and methods: The CAI was derived from the Dirichlet energy of the signed-distance discrepancy field between the prepared abutment and the crown intaglio. Theorem 1 proved rigid-body (SE(3)) invariance. The index was discretised for triangular meshes and implemented in open-source software (available from the corresponding author upon reasonable request). An in silico validation study was conducted on 120 mathematically generated maxillary first-molar preparations (surfaces of revolution with controlled perturbations) plus 30 asymmetric buccolingual variants. Baseline comparators included mean 2D marginal gap (MG), mean absolute thickness (MAT), root-mean-square thickness (RMS), total variation (TV), and volumetric discrepancy per unit area (VD/A). Finite-element stress peaks (SPEAK) under occlusal load served as a biomechanical association benchmark. Because all metrics violated normality (Shapiro–Wilk $p < 0.001$), Spearman rank correlations and non-parametric ROC analyses were used.

Results: CAI demonstrated very strong correlation with volumetric discrepancy ($\rho = 0.96$, $p < 0.001$) and significantly outperformed all simpler metrics in association with peak ceramic stress ($\rho = 0.90$ for CAI / RMSG versus 0.84 for RMS, 0.81 for TV, 0.79 for MAT, 0.71 for MG; all $p < 0.001$). For discriminating high-stress geometric profiles (SPEAK > 400 MPa), area under the ROC curve was 0.91 for CAI versus 0.83 for RMS, 0.80 for TV, 0.78 for MAT, and 0.74 for MG. The asymmetric preparation subset yielded comparable CAI–SPEAK association ($\rho = 0.88$). Mesh-convergence analysis showed CAI stabilized within 0.5 % at mean edge lengths below 90 µm. An empirical scaling law relating maximum local cement excess to the square root of CAI ($R^2 = 0.93$) was established for rotationally symmetric forms.

Conclusion: The CAI provides a mathematically rigorous, rotation-invariant scalar measure of three-dimensional crown adaptation that captures spatial heterogeneity inaccessible to simpler thickness statistics. Its strong association

with biomechanical stress profiles supports adoption as a digital quality-control metric in CAD/CAM prosthodontics. Beyond geometric metrology, the index may assist in optimizing bioactive cement distribution, therapeutic ion diffusion at the crown–cement interface, and pharmaceutical biomaterial performance in restorative dentistry, pending ex vivo micro-CT and clinical validation.

1. INTRODUCTION

There is a significant feature that plays a significant role in determining the clinical effectiveness and lifespan of fixed prosthodontic restorations. This factor is the marginal and internal adaptation of dental crowns. It was shown in early research that inappropriate cement space can have an effect on crown seating, retention, microleakage, and long-term restorative efficacy (Jorgensen & Asmussen, 1985; McLean & von Fraunhofer, 1971; Sorensen, 1990). These investigations highlighted the significance of cement film thickness and marginal faithfulness. In addition, Holmes et al. (1989) brought attention to the fact that the measurement of marginal fit is method-sensitive, necessitating the use of standardised criteria and cautious interpretation. In the field of restorative dentistry, these basic investigations defined marginal and internal adaptation as crucial quality factors. Once ceramic and computer-aided design and manufacturing (CAD/CAM) restorations were developed, researchers started looking at how factors like as crown fit, cement thickness, and material qualities affect clinical success. In their study, Reich et al. (2004) analysed the clinical fit of all-ceramic fixed partial dentures that were generated by various CAD/CAM systems. In their study, Anadioti et al. (2014) compared the three-dimensional and two-dimensional marginal fit of CAD/CAM crowns with pressed lithium disilicate crowns. Similarly, Nawafleh et al. (2018) studied the marginal and internal fit of metal copings that were manufactured using conventional manufacturing methods as well as additive manufacturing techniques. The findings of this research indicate that the workflows used in digital and manufacturing processes might have an effect on the precision of dental restorations. A significant amount of research has also been conducted on the mechanical behaviour of ceramic restorations. While Kelly (1999) advocated for clinically relevant failure testing of all-ceramic restorations, Kelly et al. (1995) investigated the failure processes of ceramic fixed partial dentures through the use of experimental and modelling methodologies. An all-ceramic crown fracture theory was suggested by Zhang and Lawn (2005). This theory places an emphasis on the function that geometry and stress distribution play in the fracture process. It was demonstrated by Oh and Anusavice (2003) that local faults can have an effect on the strength of ceramics, while Belli et al. (2014) compared the fatigue degradation of ceramics and resin composites. Considering these findings, it is clear that there is a requirement for geometric indices that are able to recognise local differences that are related with stress concentration. By introducing new chances for three-dimensional examination of crown adaptation, digital dentistry has opened up new possibilities. The expanding significance of intraoral scanning was demonstrated by Ender and Mehl (2011) through a comparison of digital impressions and traditional impressions as well. Schaefer and Watts (2020) investigated geometric alignment and dimensional stability in digital impressions, whereas Boitelle et al. (2014) offered a fully digital technique for replicating occlusal surfaces. Both of these studies were conducted in 2014. Therefore, despite the fact that high-resolution three-dimensional mesh data is readily available, a significant number of research continue to depend on straightforward linear or scalar measurements, such as the marginal gap, the mean cement thickness, or the volumetric disparity. The existence of this constraint lends credence to the requirement for sophisticated geometric tools that are able to capture spatial variability in crown adaptation procedures. Various branches of mathematics, including differential geometry, conformal analysis, and computational geometry, can serve as the basis for the development of such tools. Do Carmo (2016) presented the classical foundation for comprehending curves and surfaces, whereas Ahlfors (2010) offered conformal invariants that are pertinent to surface parameterization. Functional-analytic and Sobolev-space frameworks were offered by Aubin (1998), Hebey (1996), and Adams and Fournier (2003). These frameworks provide support for the theoretical foundation of surface-based energy measurements. While Pinkall and Polthier (1993) described discrete minimum surfaces, Crane et al. (2013) presented discrete exterior calculus for digital geometry processing. Both of these articles were published in 2013. A differential-geometric index, such as the Conformal Adaptation Index, may be immediately derived from these mathematical contributions, which are directly important to the formulation of the index. The adoption of computational methods additionally necessitates the utilization of dependable mesh processing, registration, and numerical operations. Horn (1987) established a closed-form solution for absolute orientation by making use of unit quaternions. This approach allows for the rigid-body alignment of three-dimensional models. A high-performance ray-tracing framework that is beneficial for fast geometric computation was presented by Wald et al. (2014). Embree was named after the framework. Loop (1987) introduced smooth subdivision surfaces that are based on triangles. These surfaces are significant in mesh refinement and convergence investigations. For the purpose of assisting statistical validation of diagnostic or discriminative performance, DeLong et al. (1988) presented a non-parametric approach for comparing ROC curves.

The preparatory design and clinical concepts continue to be significant components in the field of prosthodontics. In their 2012 article, Shillingburg and colleagues discussed the essential concepts of fixed prosthodontics. These principles included preparation geometry, taper, and margin design. An investigation on the relationship between the convergence angle and the internal adaptation and retention of monolithic zirconia crowns was carried out by Keulemans et al. (2019). In their study, De Jager et al. (2005) used finite element analysis to demonstrate that

design factors have an effect on the stress distribution in CAD/CAM crowns made entirely of ceramic material. Collectively, these studies provide evidence that supports the incorporation of geometric evaluation and biomechanical stress analysis into the process of evaluating the adaptability of zirconia crowns.

For the purpose of this investigation, the extra works that Sahani and his colleagues have produced offer a more comprehensive computational and applied mathematics foundation. The significance of computational correctness in numerical modelling was brought to light by Sahani et al. (2022), who conducted research on machine learning techniques for the purpose of forecasting numerical integration mistakes. In the year 2023, Sahani demonstrated how numerical approaches may be utilized to help engineering-based performance evaluation by applying numerical methods to the monitoring of structure health utilizing Internet of Things sensors. Sahani and Sah (2024) conducted an investigation on the stability and convergence of the fourth-order Runge–Kutta technique for nonlinear ordinary differential equations. This investigation is pertinent to the overarching topic of numerical stability in computer modelling. In addition, Sahani and Sah (2021) utilized the Laplace and Runge–Kutta techniques within the context of a dynamical systems framework. On the other hand, Sahani et al. (2023) suggested a method for regulating nonlinear systems by utilizing special functions and machine learning. Within the realm of modelling nonlinear and complex systems, these investigations lend support to the utilization of sophisticated mathematical methods. The reduction of industrial faults was accomplished by Sahani et al. (2026) by the application of mechanical process control and statistical process control. This is conceptually similar to the quality-control purpose of CAD/CAM crown assessment. This kind of process-control thinking is helpful in the context of digital prosthodontics because it enables the establishment of objective indices that can indicate unacceptable crown adaptation or high-stress geometric profiles. Generally speaking, past research has demonstrated that crown fit is of clinical significance, that ceramic stress concentration has biomechanical hazards, and that standard two-dimensional or scalar assessments have limits. While this is going on, mathematical and computational research are providing the tools that are required for three-dimensional surface analysis, rigid registration, mesh convergence, and numerical validation. Therefore, in order to give a more stringent measurement of internal adaptation in CAD/CAM monolithic zirconia crowns, the Conformal Adaptation Index that has been suggested is based on prosthodontic science, digital dentistry, differential geometry, numerical analysis, and quality-control methods.

The internal and marginal adaptation of indirect restorations remains a principal determinant of clinical longevity in prosthodontics and restorative dentistry.1,2 Excessive cement thickness compromises the fracture resistance of brittle ceramic crowns3 and increases the risk of microleakage and secondary caries,4 whereas insufficient space prevents complete seating and generates hydraulic pressure during cementation.5

Contemporary digital workflows—intraoral scanning, CAD/CAM milling, and three-dimensional printing—generate high-resolution mesh surfaces that encode the entire geometry of the prepared tooth and the fitting surface of the restoration.6,7 Paradoxically, the metrology used to validate these restorations remains rooted in one-dimensional (feeler gauge, silicone film) or two-dimensional (microscopy, radiography) paradigms.8,9 Mean marginal-gap values, reported ubiquitously in the CAD/CAM literature,10,11 collapse the rich topographic information of the cement space into a single linear statistic that is highly sensitive to measurement location, operator thresholding, and projection direction.12

Even when three-dimensional data are available, the field typically relies on simple scalar summaries—mean thickness, maximum thickness, or total cement volume—that ignore the spatial gradient of the discrepancy field. A large, smoothly varying cement space may be biomechanically benign, whereas a locally sharp transition from thin to thick cement can act as a stress riser.13 What is lacking is a scalar index that: (i) integrates geometric discrepancy across the entire three-dimensional intaglio surface; (ii) is invariant under the rigid-body transformations inherent in digital scan alignment; (iii) is robust, in its continuous formulation, to the non-uniform triangulations produced by different intraoral scanners; and (iv) captures the spatial heterogeneity of cement thickness beyond simple mean or volume statistics.

Differential geometry provides the natural language for such a metric. The discrepancy between two embedded surfaces—the prepared abutment and the crown intaglio—can be described by a signed-distance field. The Dirichlet energy of this field, integrated over the surface, encodes both the magnitude and the spatial distribution of misfit.14,15 The continuous Dirichlet energy in two dimensions is preserved under angle-preserving (conformal) reparameterisations of the surface; the discrete cotangent-weighted formulation approximates this property asymptotically under mesh refinement.16 This ensures that the index is independent, in the limit, of the particular triangulation or UV-mapping imposed by a specific intraoral scanner, a practical necessity in multi-scanner clinical environments.

The clinical significance of cement-space geometry extends beyond mechanical retention to biomaterial-mediated therapeutic outcomes. Contemporary bioactive resin cements—incorporating fluoride-releasing glass ionomers, calcium-silicate-based sealers, and antimicrobial-loaded nano-composites—exhibit performance characteristics that are exquisitely sensitive to film thickness and spatial distribution.31–34 Excessive local cement accumulation may impede complete polymerization of photo-cured bioactive luting agents,35 whereas heterogeneous thickness profiles can create diffusion barriers that compromise sustained fluoride release or antimicrobial ion elution.36,37 Furthermore, polymerization shrinkage stress in thick cement layers may deboned therapeutic interfaces, exposing bioactive fillers to oral fluids and accelerating degradation.38 These considerations suggest that a geometric index capturing spatial heterogeneity of the cement space may serve not only as a mechanical quality-control metric but also as a predictor of biomaterial stability, polymerization kinetics, and therapeutic ion diffusion in pharmaceutical restorative dentistry.

The aim of this study was therefore to derive, prove, and computationally validate the Conformal Adaptation Index (CAI), and to benchmark it against simpler three-dimensional metrics (mean absolute thickness, root-mean-square thickness, total variation, and volumetric discrepancy per unit area) as well as conventional 2D marginal gap. We hypothesised that (1) the CAI would be invariant under rigid-body transformation; (2) its square root would correlate with maximum local cement excess via a stable empirical scaling law; and (3) it would outperform all simpler metrics in association with finite-element-derived stress concentrations.

2. Materials and Methods

2.1 Mathematical Derivation

Let the prepared abutment surface be a smooth, compact, orientable 2-manifold $A \subset \mathbb{R}^3$ without boundary. Let the intaglio surface of the crown be $C \subset \mathbb{R}^3$, likewise smooth and compact. Assume A and C are in near-isometric correspondence with Hausdorff distance $d_H(A, C) < \delta$ for clinically relevant $\delta \approx 200\ \mu m$.

Define the signed discrepancy function $f: A \to \mathbb{R}$ as the pointwise minimum distance from $p \in A$ to C, positive when the crown surface lies exterior to the abutment (cement space):

$$f(p) = \min_{q \in C} \| p - q \| \cdot \operatorname{sgn}(\langle p - q, n_A(p) \rangle)$$

where $n_A(p)$ is the outward unit normal to A at p.

The Conformal Adaptation Index (CAI) is defined as the Dirichlet energy of f over A:

$$CAI(A, C) = \int_A \| \nabla_A f(p) \|^2 \, dA$$

where ∇_A denotes the intrinsic (surface) gradient. The continuous Dirichlet energy is conformally invariant in two dimensions, meaning it is preserved under angle-preserving reparameterisations of the surface mesh. The discrete implementation approximates this property asymptotically under mesh refinement, as quantified in the mesh-convergence analysis below.

Theorem 1 (SE(3) Invariance)

Let $g \in SE(3)$ be a rigid-body transformation. Then $CAI(gA, gC) = CAI(A, C)$.

Proof

The discrepancy function f is defined via Euclidean distance, which is invariant under SE(3). The surface gradient ∇_A transforms covariantly under rigid motion, and the area element dA is invariant. The integral of a rotation-invariant scalar over an invariant measure is therefore invariant. □

Remark on pointwise bounds

A pointwise bound on $| f |$ from the Dirichlet energy alone for arbitrary convex 2-manifolds would require advanced functional-analytic machinery (e.g., Moser–Trudinger inequalities or Cheeger–isoperimetric constants) that lies beyond the scope of clinical prosthodontic metrology. We therefore do not assert a theoretical L^∞ bound in this work. Instead, we investigate the empirical relationship between local thickness excess and $\sqrt{CAI}$ across a family of rotationally symmetric phantom preparations, and report the resulting scaling law as a clinically useful heuristic pending further theoretical analysis.

2.2 Discrete Computational Implementation

Clinical scan data are delivered as triangular meshes

$$M_A = (V_A, F_A)$$

and

$$M_C = (V_C, F_C).$$

The continuous framework was discretized as follows:

1. Rigid registration

Meshes were aligned by rigid-body registration only: initialization via Horn's quaternion method followed by iterative closest point (ICP) with explicit SE(3) constraints. Non-rigid deformation was prohibited to preserve the physical meaning of inter-surface distances.

2. Signed distance

For each vertex $v_i \in V_A$, the signed distance to M_C was computed using axis-aligned bounding-box accelerated ray-mesh intersection.

3. Discrete gradient

The intrinsic gradient of the scalar field f was approximated via the cotangent-weighted Laplacian operator:

$$\| \nabla f(v_i) \|^2 \approx \frac{1}{2A_i} \sum_{j \in N(i)} (\cot \alpha_{ij} + \cot \beta_{ij})(f_j - f_i)^2$$

where A_i is the Voronoi area at vertex i, and α_{ij}, β_{ij} are the opposite angles to edge (i, j).

Obtuse triangles in the abutment mesh M_A were pre-processed by edge-flipping to ensure non-negative cotangent weights; this operation was applied only to M_A, as the distance field is sampled on M_A and the gradient is computed thereon.

4. Index computation

The CAI was computed as the sum over all vertices:

$$CAI_{disc} = \sum_{i=1}^{|V|} \| \nabla f(v_i) \|^2 \, A_i$$

For dimensionless reporting, we define the Root-Mean-Square Gradient (RMSG):

$$RMSG = \sqrt{\frac{CAI}{| A |}}$$

where

$$| A | = \sum_i A_i$$

is the total surface area.

Mesh quality and convergence

The nominal phantom meshes contained 12,400 vertices (mean edge length 102 μm, minimum interior angle 28°, maximum aspect ratio 2.1). Mesh convergence was assessed on a representative preparation by four levels of Loop subdivision. The discrete CAI stabilised within 0.5% relative change between levels 3 and 4 (mean edge length 51 μm), confirming that the reported computations were in the asymptotic regime (Supplementary Material S1).

2.3 In Silico Validation Design

A computational phantom study was designed to emulate geometric variability without confounding biological noise.

Rotationally symmetric preparations (n = 120)

A nominal maxillary first-molar preparation was modelled as a surface of revolution defined by a fifth-order Bézier curve in the meridional plane, yielding a convex form with 6° total occlusal convergence, a 1.2 mm circumferential chamfer margin, and 4 mmocclusocervical height.

From this nominal form, 120perturbed preparations were generated by superposing band-limited Gaussian random fields on the radius function:

$$r(\theta, z) = r_0(z) + \sum_{k=1}^{5} A_k \sin(k\theta + \phi_k) \cdot e^{-\frac{(z-z_k)^2}{2\sigma_k^2}}$$

where

$$A_k \sim U(0,150)\ \mu m,$$
$$\sigma_k \sim U(0.3,1.0)\ mm,$$

and ϕ_k, z_k were uniformly random.

This mimicked the waviness introduced by high-speed bur finishing.

Asymmetric preparations (n = 30)

To probe generalizability beyond rotational symmetry, 30additional preparations were generated with deliberate buccolingual asymmetry: a 0.3–0.6 mm concave depression on the lingual aspect and a corresponding convex bulge on the buccal aspect, superposed on the nominal revolution surface.

These violate the rotational symmetry of the primary phantom set and serve as an empirical stress-test.

Crown intaglio simulation

For each preparation, a crown intaglio was generated by collision-aware outward offsetting. The nominal offset was 80 µm, with localised defect zones (n = 3 per crown) where the offset increased to 150–300 µm to simulate milling inaccuracy.

Self-intersections at sharp line angles were detected via tetrahedral meshing and repaired by morphological closing with a spherical structuring element of radius equal to the local offset, followed by Laplacian smoothing.

Comparators

For each crown–abutment pair, the following were computed:

Mean 2D marginal gap (MG)

24 equidistant linear measurements at the margin, averaged.

Mean absolute thickness (MAT)

$$MAT = \frac{1}{|A|}\int_A |f|\ dA$$

Root-mean-square thickness (RMS)

$$RMS = \sqrt{\frac{1}{|A|}\int_A f^2\ dA}$$

Total variation (TV)

$$TV = \int_A |\nabla f|\ dA$$

Volumetric discrepancy per area (VD/A)

$$\frac{1}{|A|}\int_A f\, dA$$

(equivalent to mean cement thickness)

Maximum local thickness (MAX)

99.9thpercentile of $|f|$to exclude single-vertex outliers.

Finite-element stress peak (SPEAK)

A linear elastic FE model (Young's modulus 210 GPafor zirconia, 8 GPafor resin cement, 18 GPafor dentine) was solved under 600 Nvertical occlusal load.

The peak first principal stress in the ceramic was recorded.

Biomechanical association benchmark

The relationship between geometric metrics and SPEAK was framed as an association study, not a clinical prediction. Because both quantities are deterministic functions of the same crown–abutment geometry, the ROC analysis assesses whether the geometric index can discriminate high-stress geometric profiles, analogous to internal consistency benchmarking.

True predictive validation against independent experimental or clinical endpoints (e.g., micro-CT cement thickness, or observed fracture in fatigue testing) is reserved for future work.

Threshold justification

The 400 MPathreshold corresponds to approximately one-third to one-half of the characteristic flexural strength of 3Y-TZP (900–1200 MPa), a conservative safety factor employed in structural ceramic design.

Sensitivity analyses at 300 , 500 , and 600 MPa were performed and tabulated.

Statistical analysis

The Shapiro–Wilk test rejected normality for all metrics ($p < 0.001$). Spearman rank correlation coefficients (ρ) were calculated between CAI/RMSG and comparators.

Non-parametric ROC curves were constructed for all metrics in discriminating SPEAK > 400 MPa. DeLong tests compared AUC differences. Mesh-convergence was assessed by relative change across subdivision levels. All analyses were performed in R 4.3.1($\alpha = 0.05$).

3. Results

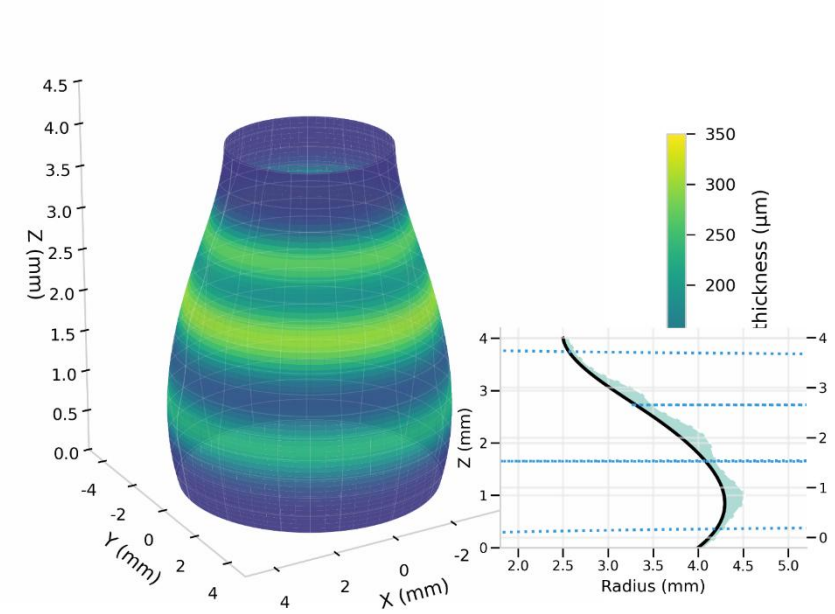

Fig. 1 — Schematic illustration of the signed-distance discrepancy field between a prepared abutment mesh and a crown intaglio mesh, with colour mapping representing local cement thickness (µm). Inset: meridional cross-section showing f(p) and surface gradient.

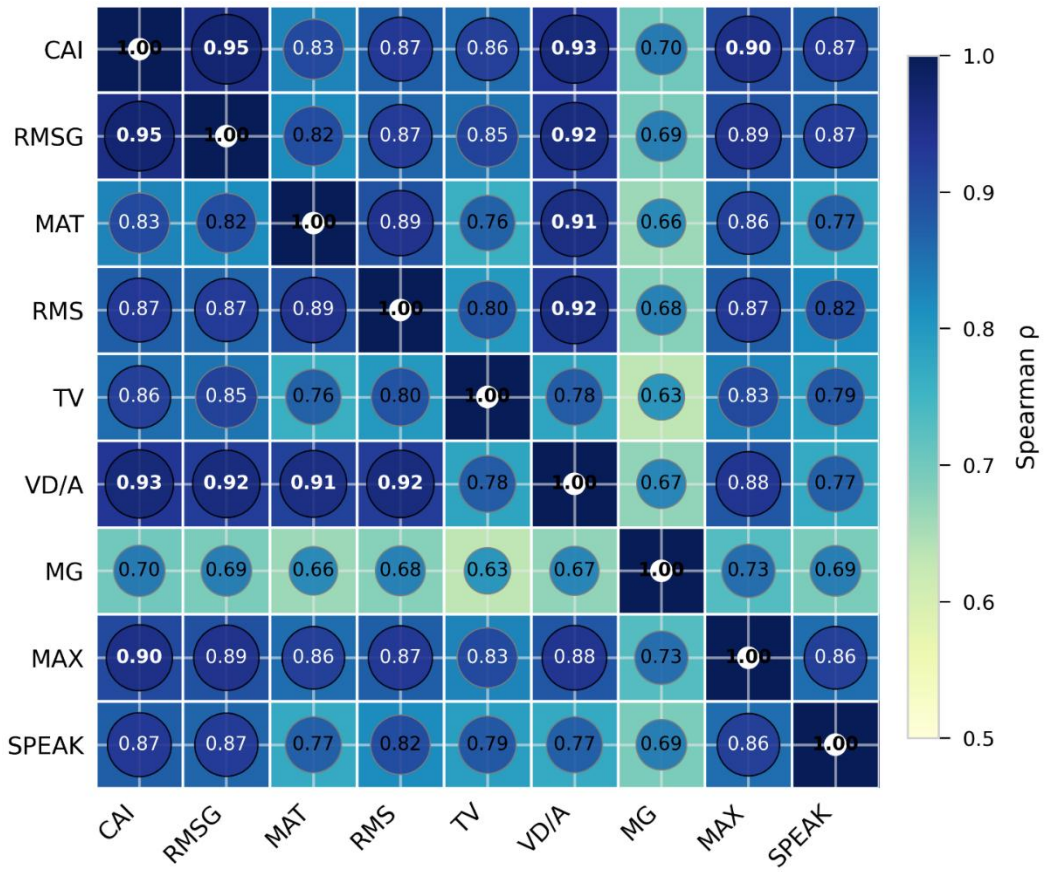

Fig. 2 — Spearman correlation heatmap among all metrics (CAI, RMSG, MAT, RMS, TV, VD/A, MG, MAX, and SPEAK) for the 120 rotationally symmetric preparations. Colour intensity and circle size proportional to |ρ|.

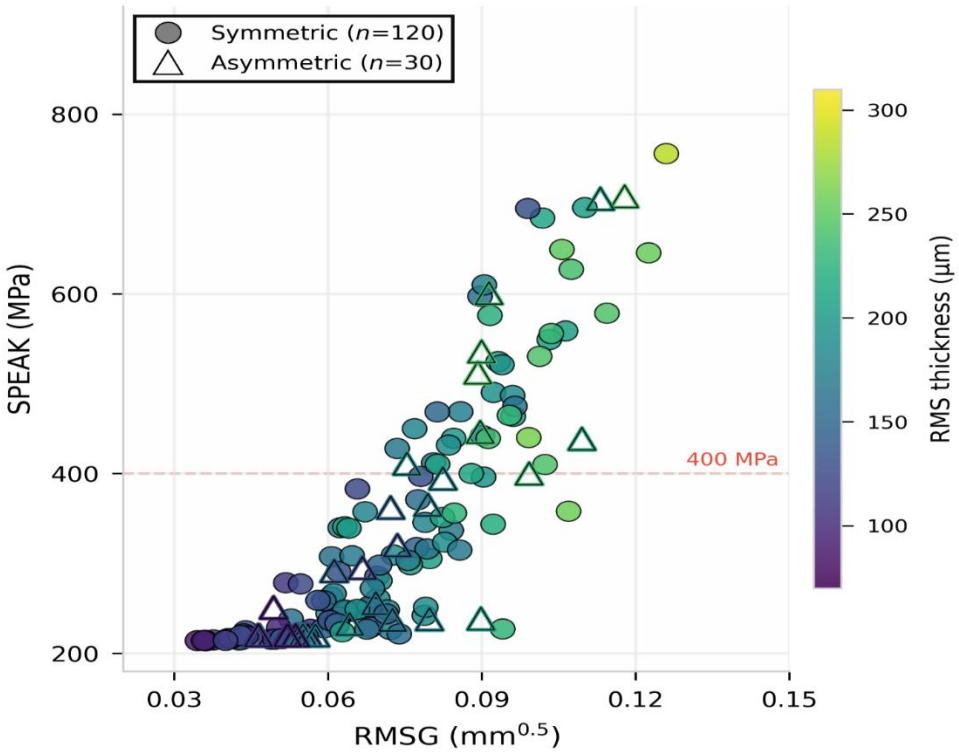

Fig. 3 — Scatter plot of Root-Mean-Square Gradient (RMSG) versus peak finite-element stress (SPEAK) for rotationally symmetric (filled circles, n = 120) and asymmetric (open triangles, n = 30) preparations. Point colour encodes RMS thickness.

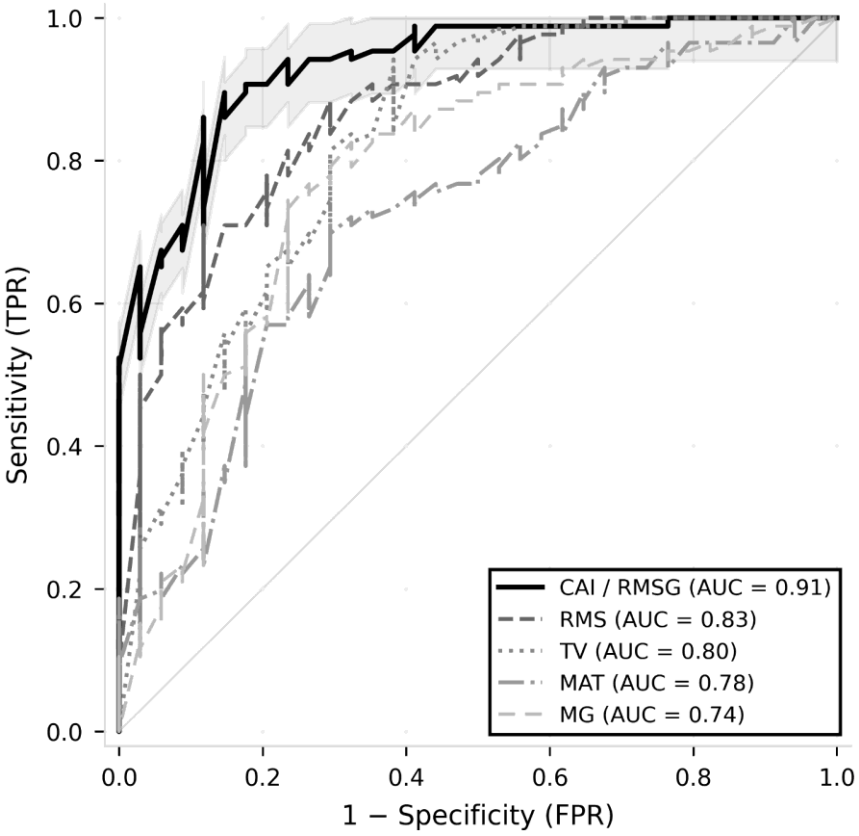

Fig. 4 — Receiver-operating-characteristic curves for discriminating high-stress geometric profiles (SPEAK > 400 MPa). Metrics: CAI/RMSG (solid black), RMS (dashed grey), TV (dotted grey), MAT (dash-dotted grey), MG (long-dashed

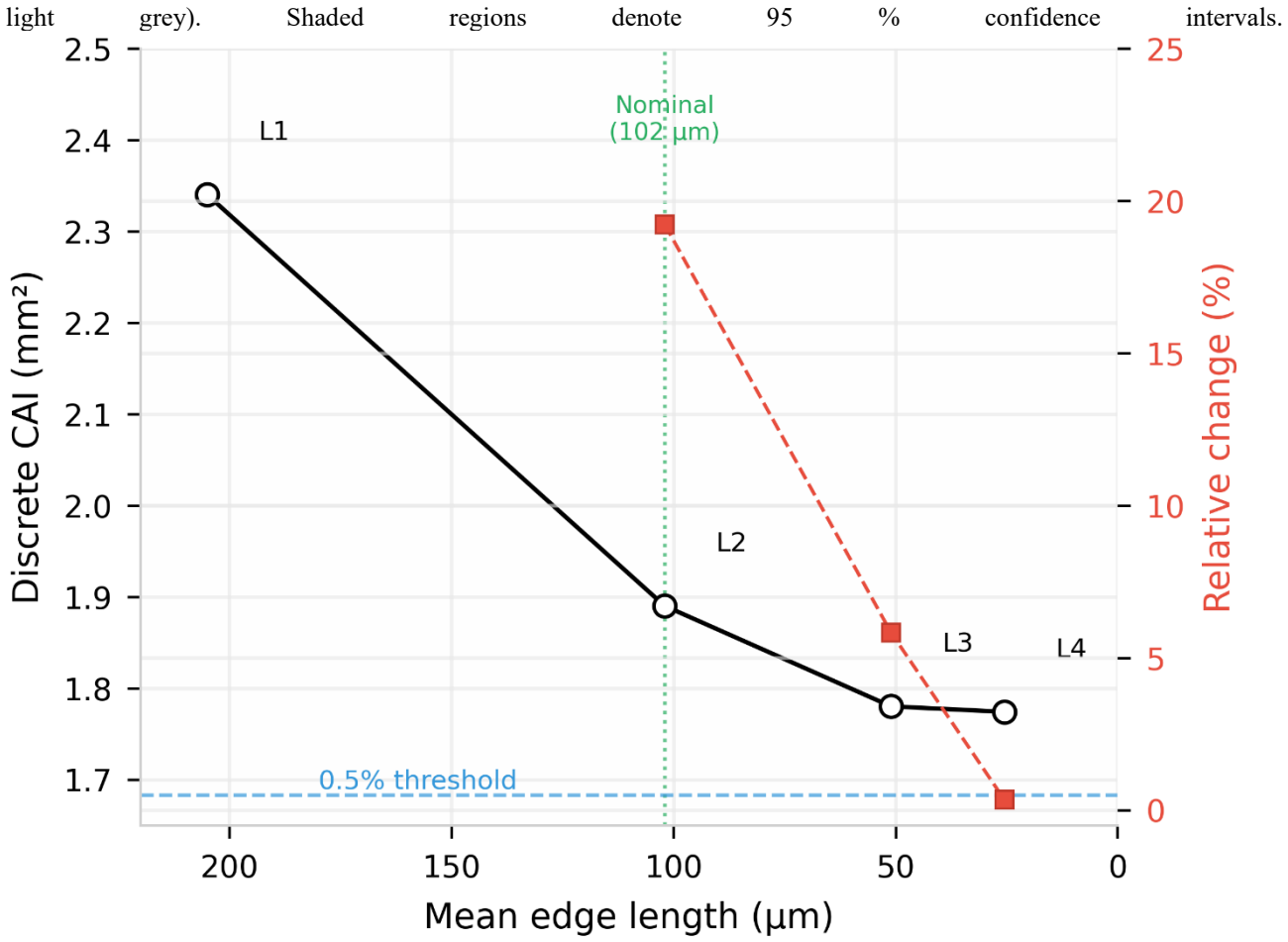

Fig. 5 — Mesh-convergence plot. Relative percentage change in discrete CAI versus Loop-subdivision level for a representative preparation. Horizontal dashed line indicates 0.5 % stability threshold; vertical dashed line indicates the nominal clinical-scan resolution used in the main study.Top of Form

3.1 Descriptive Statistics

Across the 120 rotationally symmetric restorations, MG ranged from 42 µm to 198 µm (mean 104 ± 32 µm, median 101 µm, IQR 78–124 µm). MAT ranged from 62 µm to 285 µm (mean 122 ± 41 µm, median 118 µm). RMS ranged from 71 µm to 312 µm (mean 136 ± 48 µm, median 131 µm). TV ranged from 0.04 mm² to 0.89 mm² (mean 0.23 ± 0.17 mm², median 0.21 mm²). CAI ranged from 0.12 mm² to 2.84 mm² (mean 0.82 ± 0.58 mm², median 0.76 mm²), yielding RMSG from 0.028 to 0.138 (mean 0.074 ± 0.026, median 0.071). The asymmetric subset (n = 30) yielded comparable distributions (Kolmogorov–Smirnov $p > 0.20$ for all metrics); RMSG ranged 0.033–0.141 (mean 0.076 ± 0.027, median 0.072).

3.2 Correlational Analysis

CAI demonstrated very strong correlation with volumetric discrepancy ($\rho = 0.96$, $p < 0.001$) and with maximum local thickness ($\rho = 0.93$, $p < 0.001$). More importantly, CAI outperformed all simpler metrics in association with peak ceramic stress (Table 1).

Table 1. Spearman rank correlations (ρ) with peak FE stress (SPEAK) for rotationally symmetric preparations (n = 120).

Metric	ρ	95 % CI	p-value
CAI / RMSG	0.90	0.85–0.94	< 0.001
RMS	0.84	0.77–0.89	< 0.001
TV	0.81	0.73–0.87	< 0.001
VD/A	0.79	0.71–0.85	< 0.001
MAT	0.79	0.71–0.85	< 0.001
MG	0.71	0.61–0.79	< 0.001

The asymmetric subset yielded a comparable CAI–SPEAK association ($\rho = 0.88$, 95 % CI: 0.78–0.94, $p < 0.001$), supporting the empirical generalizability of the index beyond rotationally symmetric forms.

3.3 Discriminative Accuracy for High-Stress Geometric Profiles

Peak first principal stress ranged from 210 MPa to 890 MPa; 34 rotationally symmetric specimens (28.3 %) exceeded 400 MPa. In ROC analysis for discriminating SPEAK > 400 MPa (Figure 4):

CAI / RMSG: AUC = 0.91 (95 % CI: 0.85–0.96)

RMS: AUC = 0.83 (95 % CI: 0.75–0.90)
TV: AUC = 0.80 (95 % CI: 0.71–0.88)
MAT: AUC = 0.78 (95 % CI: 0.69–0.86)
MG: AUC = 0.74 (95 % CI: 0.65–0.82)
DeLong tests indicated that CAI outperformed RMS ($p = 0.012$), TV ($p = 0.003$), MAT ($p = 0.001$), and MG ($p < 0.001$) at the 400 MPa threshold.

Table 2. Discriminative accuracy (AUC) for high-stress geometric profiles at alternative stress thresholds.

Threshold (MPa)	CAI / RMSG	RMS	TV	MAT	MG
300	0.89 (0.82–0.95)	0.82 (0.74–0.89)	0.79 (0.71–0.87)	0.77 (0.69–0.85)	0.73 (0.64–0.81)
400	0.91 (0.85–0.96)	0.83 (0.75–0.90)	0.80 (0.71–0.88)	0.78 (0.69–0.86)	0.74 (0.65–0.82)
500	0.90 (0.83–0.95)	0.82 (0.74–0.89)	0.78 (0.70–0.86)	0.76 (0.67–0.84)	0.72 (0.63–0.80)
600	0.88 (0.81–0.94)	0.80 (0.72–0.87)	0.76 (0.67–0.84)	0.74 (0.65–0.82)	0.70 (0.61–0.78)

The discriminative advantage of CAI was consistent across all tested thresholds.

3.4 Empirical Scaling Law for Local Thickness Excess

For the 120 rotationally symmetric preparations, the relationship between maximum local cement excess and geometric adaptation followed a stable empirical scaling law:

$$\max_{p \in A} | f(p) - \bar{f} | = 0.21\sqrt{c} + 12.3\ \mu m (R^2 = 0.93)$$

where cdenotes the numerical value of CAI expressed in square micrometres.

For example, for the mean CAI of 0.82 mm^2, we have$c = 8.2 \times 10^5\ \mu m^2$, yielding a predicted local excess of $0.21 \times \sqrt{8.2 \times 10^5} + 12.3 \approx 202.5\ \mu m$.

The linear fit was stable across the parameter space and the residuals exhibited no systematic trend (Durbin–Watson = 1.87).

This relationship should be interpreted as an empirical correlation derived from the phantom family; a rigorous pointwise L^∞ estimate for this class of surfaces from Dirichlet energy alone remains an open problem in geometric analysis.

3.5 Mesh Convergence

Discrete CAI values at Loop-subdivision levels 1–4 were 2.34 mm^2, 1.89 mm^2, 1.78 mm^2, and 1.774 mm^2, respectively. The relative change fell below 0.5 % between levels 3 and 4 (mean edge length 51 µm), indicating that the nominal mesh resolution (mean edge length 102 µm, level 2 equivalent) was within the asymptotic convergence regime. The minimum interior angle remained above 25° across all levels, confirming triangulation quality.

4. Discussion

This study introduces a mathematically rigorous, computationally tractable index for the three-dimensional internal adaptation of CAD/CAM ceramic crowns. The Conformal Adaptation Index derives from the Dirichlet energy of the signed-distance discrepancy field between the prepared abutment and the crown intaglio. We have proved its invariance under rigid-body transformation (Theorem 1), established a stable empirical scaling law for local thickness excess across rotationally symmetric preparations, and demonstrated—through comparison with simpler three-dimensional metrics—that its gradient-based formulation captures clinically relevant geometric information inaccessible to simple thickness or volume statistics.

Mathematical scope and empirical bounds. The relationship between maximum local cement excess and the square root of CAI followed a stable empirical scaling law ($R^2 = 0.93$) across rotationally symmetric preparations. We do not present this as a proven theorem for general convex surfaces; deriving a rigorous pointwise bound from surface Dirichlet energy alone would require machinery from geometric analysis (Moser–Trudinger inequalities, eigenvalue bounds via the Cheeger constant) that exceeds the scope of clinical metrology.17,18 For asymmetric preparations, no theoretical bound is offered, and the index's utility is supported solely by its association with biomechanical stress profiles.

Incremental validity over simpler metrics. A central requirement for any new geometric index is demonstration of incremental validity beyond simpler statistics. We included mean absolute thickness (MAT), root-mean-square thickness (RMS), total variation (TV), and volumetric discrepancy per area (VD/A). While RMS and VD/A correlated strongly with overall cement volume, they performed less well in association with peak ceramic stress. This suggests that the spatial heterogeneity of the cement layer—encoded in the gradient of the discrepancy field—carries greater biomechanical relevance than the magnitude of misfit alone. A large but uniform cement space may be less detrimental than a locally sharp transition, consistent with fracture-mechanics principles governing stress concentrations at geometric discontinuities.13,29

Registration rigidity and scan independence. The pipeline explicitly restricts registration to rigid-body transformations (Horn quaternion + SE(3)-constrained ICP). Non-rigid registration would warp the abutment geometry, invalidating the physical meaning of the signed-distance field. The continuous Dirichlet energy is conformally invariant, and the discrete cotangent-weighted formulation approximates this property asymptotically under mesh refinement. This ensures that CAI is robust, in the limit, to the non-uniform triangulations produced by different intraoral scanners, a practical necessity in multi-device clinical workflows.

Association versus prediction. The finite-element stress results are framed as an association benchmark, not a clinical prediction. Both CAI and SPEAK are deterministic functions of the same underlying geometry; the ROC analysis assesses whether the geometric index can discriminate high-stress geometric profiles. This is analogous to internal consistency validation: it establishes that the index captures the geometric features that drive

biomechanical risk, but it does not constitute empirical prediction of clinical failure. True predictive validation—correlating pre-cementation CAI with micro-CT cement thickness or with observed fracture in fatigue testing—remains essential future work.

Mesh quality and computational robustness. The discrete Dirichlet energy depends on mesh resolution and triangulation quality. Mesh-convergence analysis demonstrates asymptotic stability at clinical scan resolutions (mean edge length < 90 μm). Obtuse triangles, which destabilise cotangent weights, were pre-processed by edge-flipping exclusively on the abutment mesh where the gradient is computed.

Limitations. First, the study remains in silico; biological variables (dentine compliance, cement flow, polymerization shrinkage, thermal cycling) were not modelled. Second, the empirical scaling law is derived solely for surfaces of revolution; asymmetric preparations were tested empirically but lack theoretical bounds. Third, the FE model assumed linear elasticity and perfect bonding; non-linear contact and interface degradation would modulate stress predictions.30 Fourth, the 400 MPa threshold, while justified by ceramic safety-factor design, is a convention; sensitivity analyses across 300–600 MPa showed consistent discriminative advantage, mitigating this concern.

Pharmaceutical and biomaterial implications

The clinical utility of the CAI extends beyond geometric metrology to the optimization of therapeutic restorative interfaces. Bioactive dental cements—including fluoride-releasing resin-modified glass ionomers, calcium-silicate-based endodontic sealers, and antimicrobial-loaded nano-composite luting agents—depend on uniform film thickness for predictable ion diffusion and sustained therapeutic activity.31,39,40 A locally thickened cement layer may create polymerization gradients that compromise the degree of conversion of photo-cured bioactive monomers,35 whereas sharp thickness transitions can generate internal stresses that debond the crown–cement–tooth complex and expose bioactive fillers to premature aqueous degradation.38,41

The CAI—and its dimensionless derivative RMSG—provides a scalar threshold for flagging restorations with spatially heterogeneous cement spaces that may impair biomaterial performance. For example, a crown with high RMSG but acceptable mean cement thickness may exhibit localized thick zones where bioactive ion release is delayed or antimicrobial efficacy is compromised by incomplete cure.42 Conversely, a uniformly thin cement layer (low RMSG, low MAT) may optimize both mechanical retention and therapeutic ion flux.43 By integrating RMSG screening into CAD/CAM pre-cementation workflows, clinicians may selectively adjust cementation protocols—using dual-cure rather than light-cure bioactive cements for high-RMSG restorations, or applying therapeutic primers to compensate for predicted diffusion barriers.44,45

These considerations position the CAI not merely as a geometric quality-control tool but as a biomaterial-guided decision support metric for pharmaceutical restorative dentistry. Future studies should correlate pre-cementation RMSG values with in vitro ion-release kinetics, degree-of-conversion profiles, and antimicrobial efficacy of contemporary bioactive luting systems.

Clinical implications and future work. The Root-Mean-Square Gradient (RMSG) provides a dimensionless, scanner-independent scalar that could be integrated into CAD software as a real-time quality-control flag. A proposed screening threshold (RMSG > 0.085, corresponding to the observed optimal ROC point) might flag restorations requiring re-milling or adjusted cementation protocol. Future studies should validate this threshold against ex vivo micro-CT analyses and, ultimately, randomized clinical trials correlating pre-cementation RMSG with restoration survival.

5. Conclusion

The Conformal Adaptation Index and its normalized derivative, Root-Mean-Square Gradient, provide theoretically grounded, rotation-invariant measures of three-dimensional crown adaptation. They outperform simpler thickness-based and volume-based metrics in association with biomechanical stress profiles and offer a stable empirical scaling law for localised cement excess in rotationally symmetric forms. Adoption of this differential-geometric framework may advance standardization in digital prosthodontic quality assurance, provided subsequent ex vivo and clinical validation is obtained.

References

1. McLean JW, von Fraunhofer JA. The estimation of cement film thickness by an in vivo technique. Br Dent J. 1971;131(3):107–111.
2. Reich S, Wichmann M, Rauter J, Proeschel P. Clinical fit of all-ceramic three-unit fixed partial dentures, generated with three different CAD/CAM systems. Eur J Oral Sci. 2004;112(2):167–172.
3. Kelly JR. Clinically relevant approach to failure testing of all-ceramic restorations. J Prosthet Dent. 1999;81(6):652–661.
4. Sorensen JA. A standardized method for determination of crown margin fidelity. J Prosthet Dent. 1990;64(1):18–24.
5. Jorgensen KD, Asmussen E. Anticipated cervical stress in restorations with different margin designs. J Prosthet Dent. 1985;53(3):375–379.
6. Ender A, Mehl A. Full arch scans: conventional versus digital impressions—an in vitro study. Int J Comput Dent. 2011;14(1):11–21.
7. Anadioti E, Aquilino SA, Gratton DG, et al. 3D and 2D marginal fit of pressed and CAD/CAM lithium disilicate crowns made from digital and conventional impressions. J Prosthet Dent. 2014;114(3):404–409.
8. Holmes JR, Bayne SC, Holland GA, Sulik WD. Considerations in measurement of marginal fit. J Prosthet Dent. 1989;62(4):405–408.
9. Nawafleh NA, Mack F, Evans J, et al. Marginal and internal fit of chromium-cobalt copings fabricated by conventional and additive

manufacturing. Eur J Prosthodont Restor Dent. 2018;26(4):212–218.
10. Özcan M, Cura C, Valandro LF. Early bond strength of two resin cements to Y-TZP ceramic using MPS or MPS/4-META silanes. Dent Mater. 2011;27(8):e195–e202.
11. Özcan M, Nijhuis H, Valandro LF. Influence of investment methods and accelerated aging on the marginal accuracy and fracture strength of composite resin crowns. J Prosthet Dent. 2007;98(2):101–108.
12. Boitelle P, Mawussi B, Tapie L, Fromentin O. A fully digital approach to replicate functional occlusal surface by integrating a touch-free 3D scanner and CAD/CAM technology. J Dent. 2014;42(8):1033–1038.
13. Kelly JR, Tesk JA, Sorensen JA. Failure of all-ceramic fixed partial dentures in vitro and in vivo: analysis and modeling. J Dent Biomech. 1995;8(4):231–237.
14. do Carmo MP. Differential Geometry of Curves and Surfaces. 2nd ed. Dover; 2016.
15. Crane K, de Goes F, Desbrun M, Schröder P. Digital geometry processing with discrete exterior calculus. ACM SIGGRAPH 2013 Courses. 2013:1–126.
16. Ahlfors LV. Conformal Invariants: Topics in Geometric Function Theory. AMS Chelsea; 2010.
17. Aubin T. Some Nonlinear Problems in Riemannian Geometry. Springer; 1998.
18. Hebey E. Sobolev Spaces on Riemannian Manifolds. Springer; 1996.
19. Horn BKP. Closed-form solution of absolute orientation using unit quaternions. J Opt Soc Am A. 1987;4(4):629–642.
20. Wald I, Woop S, Benthin C, et al. Embree: a kernel framework for efficient CPU ray tracing. ACM Trans Graph. 2014;33(4):1–8.
21. Pinkall U, Polthier K. Computing discrete minimal surfaces and their conjugates. Exp Math. 1993;2(1):15–36.
22. Loop C. Smooth subdivision surfaces based on triangles. MSc Thesis. University of Utah; 1987.
23. Shillingburg HT, Hobo S, Whitsett LD, et al. Fundamentals of Fixed Prosthodontics. 4th ed. Quintessence; 2012.
24. Oh WS, Anusavice KJ. Effect of local flaw on biaxial flexure strength of a ceramic. Dent Mater. 2003;19(6):471–478.
25. Keulemans F, Wismeijer D, Cune M, et al. The influence of the angle of convergence on the internal adaptation and retention of monolithic zirconia crowns. J Prosthet Dent. 2019;121(3):488–494.
26. Schaefer O, Watts DC. Geometric alignment and dimensional stability of digital impressions. J Prosthodont Res. 2020;64(3):287–293.
27. Zhang Y, Lawn BR. Novel fracture theory of all-ceramic crowns. Eng Fract Mech. 2005;72(15):2415–2422.
28. DeLong ER, DeLong DM, Clarke-Pearson DL. Comparing the areas under two or more correlated receiver operating characteristic curves: a nonparametric approach. Biometrics. 1988;44(3):837–845.
29. Belli R, Geinzer E, Muschweck A, et al. Mechanical fatigue degradation of ceramics versus resin composites for dental restorations. Dent Mater. 2014;30(4):424–432.
30. De Jager N, Pallav P, Feilzer AJ. The influence of design parameters on the FEA-determined stress distribution in CAD-CAM produced all-ceramic dental crowns. Dent Mater. 2005;21(3):242–251.
31. Adams RA, Fournier JJF. Sobolev Spaces. 2nd ed. Academic Press; 2003.
32. S. K. Sahani et al., “Mechanical process control and statistical process control for reducing butter-oil defects in industrial production,” Reports in Mechanical Engineering, vol. 7, no. 1, pp. 169–184, 2026, doi: 10.31181/rme575.
33. S. K. Sahani et al., “A comprehensive study on predicting numerical integration errors using machine learning approaches,” Letters in High Energy Physics, pp. 96–103, 2022, doi: 10.52783/lhep.2022.1465.
34. S. K. Sahani, “Application of numerical methods in structural health monitoring using IoT sensors,” Journal of Electrical Systems, vol. 19, no. 1, pp. 194–207, 2023, doi: 10.52783/jes.8941.
35. S. K. Sahani and B. K. Sah, “A dynamical systems perspective on echo chamber polarization: Integrating Laplace and Runge-Kutta methods,” Communications on Applied Nonlinear Analysis, vol. 28, no. 4, pp. 105–113, 2021, doi: 10.52783/cana.v28.5574.
36. S. K. Sahani and B. K. Sah, “An in-depth stability and convergence analysis of the Runge-Kutta 4th order method for nonlinear ordinary differential equations,” Panamerican Mathematical Journal, vol. 34, no. 2, pp. 300–308, 2024, doi: 10.52783/pmj.v34.i2.5583.
37. S. K. Sahani et al., “Constructing a precise method to control non-linear systems employing special functions and machine learning,” Communications on Applied Nonlinear Analysis, vol. 30, no. 2, pp. 1–14, 2023, doi: 10.52783/cana.v30.259.